High-precision RTK Positioning with Tilt Compensation: Data Fusion Algorithm

Huan Lin, *Wuhan University*

BIOGRAPHY

Huan Lin Huan Lin received the B.Eng. degree in Geodesy and Survey Engineering from Wuhan University, Wuhan, China, in 2019. She is currently a Master student in the GNSS Research Center, Wuhan University, Wuhan, China. Her research interests focus on INS with aiding and its applications in geodesy and precise surveying engineering.

ABSTRACT

Global navigation satellite system (GNSS) real-time kinematic (RTK) positioning with tilt compensation breaks the conventional positioning pattern with level-free and tilted surveys. The inertial measurement unit (IMU)-based solution uses mainstream tilted RTK principles, but it is disturbed by inertial navigation system (INS) alignment and degraded performance with increasing tilt angle. This solution has been applied to the GNSS receivers of some companies. However, there are few relevant literature reports, and technical details are not available. In this paper, we propose a low-cost and efficient IMU-based tilted RTK solution with relevant algorithms, including a rapid and accurate heading alignment method and zero velocity update (ZUPT) with lever arm compensation. The proposed heading alignment method calculates the initial heading from the angle between INS-indicated and RTK-indicated trajectories. An INS updating algorithm distinguished from conventional one is used to obtain INS-indicated trajectories by treating the pole movement as rigid body motion and discarding accelerometer measurement. ZUPT with lever arm compensation doesn't require the pole to keep completely still. This ZUPT works when the pole tip touchs the ground. By validating the zero velocity of the pole tip, we can constrain the position error divergence and reduce the defects of the tilt angle. Then, accuracy analysis is performed, and explicit error equations are obtained. Experiments are carried out to validate the proposed solution, and the statistical results indicate that 1) the initial heading can be accurately determined to be 1.15° at a 98.2% confidence level within 2∼3 seconds; 2) taking the ratio of horizontal error within 2 cm as a criterion, ZUPT with lever arm compensation can raise this ratio effectively even at a large tilt angle; 3) the horizontal position error of the proposed tilted RTK solution is within 2 cm at a 96.97% confidence level at a normal tilt angle.

I. INTRODUCTION

Real-time kinematic (RTK) positioning is a mature and proven measurement technology, that is widely used in high-precision dynamic field surveys. To optimize the reception of the global navigation satellite system (GNSS) signal, the antenna is usually mounted on the top of a measurement pole, hereafter referred to as the pole, and the pole tip is fixed on the target point during the survey. In traditional RTK positioning, the pole needs to be leveled with a circular bubble, to ensure that the pole is held vertically. Only in this case, can the position of the antenna phase center (APC) measured by RTK positioning be reduced to the pole tip by taking into consideration the phase center offset (PCO) and the pole length.

Conventional RTK solutions have several apparent defects limiting the surveying efficiency, accuracy and applicability [1]. First, leveling the pole requires a time-consuming procedure to make the level bubble remain stable within a small circle, resulting in great losses in efficiency. Second, when the surveyor manually adjusts the pole to vertical, the subsequent survey performance is influenced by human operational errors and instrumental imperfections. Third, in some application scenarios, it is difficult and even impossible to hold the pole vertically on the point of interest, such as building corners, steep slope positions and obstructed points. As a result, tilted GNSS RTK positioning, (hereafter referred to as tilted RTK) has emerged, in which the pole is creatively level-free and the pole can be tilted during survey [2], as illustrated in Fig 1. This approach overcomes the operational inconvenience mentioned above and extends the applicability of RTK positioning especially in restrictive environments.

The existing tilted RTK solutions can typically be divided into three types [3]: the magnetometer-based approach, the resection-based approach and the inertial measurement unit (IMU)-based approach. The magnetometer-based approach determines the roll and pitch from an accelerometer and obtains the heading from a calibrated magnetometer. In the early commercialization of tilted RTK, most companies applied this approach to their GNSS receiver, such as S10 produced by Guangzhou STONEX Surveying and Mapping Technology Co., Ltd., Guangzhou, China. The resection-based approach adopts conventional resection technology in which the coordinates of an unknown target point should be determined by multiple measurements of surrounding points. Therefore, the surveyor is supposed to perform tilted surveys in different directions. The position of the target point is usually computed by the least squares method. Both the iRTK5 receiver from Hi-Target Surveying Instrument Co., Ltd.,

Guangzhou, China and Trimble R10 from Trimble Inc., Sunnyvale, California, USA, are based on this approach. The IMU-based approach is similar to the first approach, as it obtains the roll and pitch through an accelerometer. However, the heading is derived from inertial sensors and is independent from magnetometers. A large proportion of the latest tilted RTK receivers optimize their tilted RTK solution with this approach, such as Hi-Target iRTK5X and Leica GS18 T [4] from Leica Geosystems AG Ltd., Switzerland.

The biggest problem of the magnetometer-based approach is that the magnetometer is vulnerable to magnetic disturbance. This method is disturbed by metallic objects, such as vehicles, iron fences and beams or even reinforced concrete, all of which are often found on construction sites. This drawback leads to a lack of accuracy and robustness. Moreover, the magnetometer requires not only onsite calibration at each field survey but also frequent recalibration as the distance increases even during the same operation, which is tedious and inefficient. The resection-based approach makes the former approach free of instrumental calibration, and its mathematical model is mature and reliable. However, to approach optimized values, multiple tilted measurements for one target and good geometric structure of observations are required, leading to tedious operation and low efficiency. By contrast, the IMU-based approach performs better. The latter approach has gradually taken the place of other methods in the mainstream, benefiting from rapidness, accuracy and robustness. First, it is calibration-free and multimeter-free, which can increase the operational efficiency. Second, sensor fusion in GNSS and inertial navigation system (INS) can make full use of information, thus benefiting positioning performance in difficult conditions such as urban canyons. Third, this approach is totally immune to magnetic disturbances caused by ferrous metals and electric currents, both of which are usually present in RTK field survey environments.

However, there are still difficulties in the IMU-based approach. First, a large tilt angle impairs the RTK performance. In this scenario, the antenna starts to lose track of some satellites and the APC becomes unstable [1]. To minimize this confusion, many companies have focued on enhancing signal tracking and capture technologies [1], such as increasing the number of channels, and innovating the signal capture technology. Moreover, the accuracy of tilted compensation declines as the tilt increases since the same attitude error has a higher impact on the survey with a larger tilt angle. Thus, it is vital to guarantee the attitude precision at an acceptable level in tilted compensation. Second, the IMU-based approach encounters difficulties in heading alignment. Traditionally, there are three heading alignment solutions [5–7]: self-alignment by a gyroscope, external information aid, and in-motion alignment. Self-alignment on a fixed platform requires aviation-grade gyros or better [8], which is not feasible for the low-cost IMUs in tilted RTK receivers. External information aids usually uses magnetometers or multiple-antenna GNSS equipment [9]. However, the former is sensitive to magnetic disturbance, and the latter is not practical for portable RTK receivers. In-motion alignment usually requires fast movement or various dynamics, such as tilted RTK receivers X12 and i90 from Shanghai HUACE Navigation Technology Ltd., Shanghai, China, which require a movement of approximately 15 to 30 m and dozens of seconds to complete initialization, which is tedious and time consuming.

In the following section, we focus on the IMU-based tilted RTK solution. This solution has been applied to mass-producting GNSS receivers in some companies. However, papers on tilted RTK are few. Relevant information is limited to companies'websites, product manuals and patents. Technical details on the key algorithms are not available. Based on the background above, this paper is dedicated to a novel tilted RTK solution with fast alignment and lever arm compensating zero velocity update (ZUPT). We devise a rapid and accurate INS alignment method implemented through wiggling the pole over two or three seconds. This proposed in-motion alignment method is easy to use and time efficient than the previous methods, as well as sufficiently accurate, with heading errors less than 1.15° at a 98.2% confidence level. Moreover, ZUPT with lever arm compensation in this scheme can validate the zero velocity of the pole tip, thus effctively reducing the effect of the tilt angle. The accuracy of our tilt compensation is 2 cm horizontally at a 95.25% confidence level with a 30° tilt angle, which is desirable for low-cost IMU-based tilted RTK equipment.

II. METHODOLOGY

In our tilted RTK equipment, the navigation integrated system (including a MEMS IMU chip) and GNSS antenna is equipped on the pole top, as illustrated in Fig 4. In practice, the surveyor uses this equipment to perform tilted surveys. The operation flow is summarized below:

(1) Power on the equipment, lay it down and keep it still for 2∼3 minutes. This operation is required in a new power-on to remove large gyro bias from MEMS IMU measurement.

(2) Perform alignment motions. As illustrated in Fig 3, tilt the pole at an arbitrary position A and remain still for 2 seconds; and then wiggle the pole to the position B within 2∼3 seconds. This wiggle is recomended to repeat several times.

(3) Perform tilted RTK surveys. For every target points, fix the pole tip on the point for several seconds. Carry the pole and walk to the next point when the survey at one point is finshed. Destinguish from the conventional RTK, tilted RTK doesn't require the surveyor to level the pole and hold it stationary at each point. Tilt and wiggle are allowable as long as the pole tip is fixed. But we advise the surveyor to hold the pole with slight tilt on normal points, because a large tilt

angle (>30°) impairs the performance of GNSS receivers.

(4) Power off the equipment after the measurement.

The algorithm scheme of our tilted RTK solution is shown in Fig 2. Two sensors (MEMS IMU and GNSS RTK receiver) and four main alogorithm modules (INS mechanization, initial alignment, integration Kalman filter and tilt compensation) are highlighted in boxes. Key transmit information is marked follow the arrows. INS mechanization is a mature INS reckoning algorithm that can be found in [10]. Arrow (1) pointing to initial alignment is in dotted line means that 1) this alignment module only works when lack of initial navigation values; 2) if the heading accuracy cannot meet the requirement during surveys due to heading divergence, we can restart this alignment module to obtain an accurate heading. Zero Velocity of the pole tip is used in Kalman filter to enable ZUPT with lever arm compensation. The dotted arrow (2) shows that this ZUPT only works when the pole tip touchs the ground. The position of the IMU center from Kalman filter is used in tilt compensation to obtain the position of the pole tip, as illustrated in arrow (3). In some IMU-based tilted RTK solutions, the APC position from RTK positioning is used in tilt compensaion. There is no particular benefit to using one style over the other, but putting the position from Kalman filter into tilt compensation makes the positioning robuster.

Note that there are three different positions in our algorithm scheme: the pole tip, the IMU center and the APC. The pole tip position is the target point position. And the IMU center is assumed to coincide with the APC in the following for analysis convenience, hereafter collectively referred to as the IMU center unless otherwise stated.

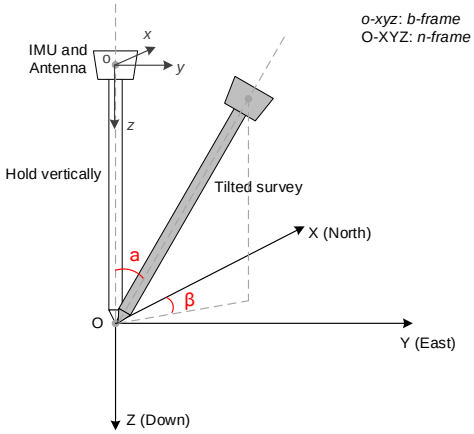

Figure 1: Illustration of tilted RTK positioning. Tilt angle α is defined as the angle between the vertical direction and the tilted pole, and horizontal azimuth β is defined as the angle between north and the plane projection of the tilted pole. The IMU center is assumed to coincide with the APC for analysis convenience.

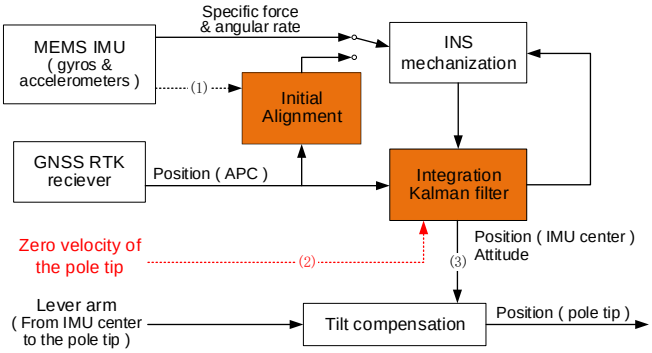

Figure 2: Basic data processing schematic of the proposed tilted RTK solution. An error-state loosely coupled Kalman filter is applied in the proposed solution. But INS correction is not shown for simplicity.

1. Tilt Compensation in the IMU-based Tilted RTK solution

The principle of tilt compensation is straightforward: the position of the pole tip is calculated from the IMU center position by considering lever arm correction, as follows

$$\boldsymbol{r}_T^n = \boldsymbol{r}_I^n + \mathbf{D}_R^{-1}\mathbf{C}_b^n \boldsymbol{l}^b \tag{1}$$

where $\boldsymbol{r}_T^n$ and $\boldsymbol{r}_I^n$ are the position vectors of the pole tip and the IMU center, respectively, resolved in the local geographic north-east-down frame, *i.e.*, the *n*-frame. Note that the position is expressed in the form of latitude φ, longitude λ and height h. Here, $\boldsymbol{l}^b$ is the level arm vector from the IMU center to the pole tip in the IMU sensor frame, i.e., the forward-right-down *b*-frame, as depicted in Fig 1. $\mathbf{D}_R^{-1} = \mathrm{diag}(\begin{bmatrix} \frac{1}{R_M+h} & \frac{1}{(R_N+h)\cos\varphi} & -1 \end{bmatrix}^{\mathrm{T}})$ is a diagonal matrix that converts the delta position from meters to delta latitude in radian and deleta height in meter, where R_M and R_N are respectively the meridian and transverse radii of curvature. $\mathbf{C}_b^n$ is the *b*-frame to *n*-frame transformation matrix, which can be calculated in terms of the successive Euler angles: heading ψ, pitch θ and roll ϕ.

$$\mathbf{C}_b^n = \begin{bmatrix} c\theta c\psi & -c\phi s\psi + s\phi s\theta c\psi & s\phi s\psi + c\phi s\theta c\psi \\ c\theta s\psi & c\phi c\psi + s\phi s\theta s\psi & -s\phi c\psi + c\phi s\theta s\psi \\ -s\theta & s\phi c\theta & c\phi c\theta \end{bmatrix} \tag{2}$$

where *c* and *s* refer to the cosine and sine operators, respectively.

The above equation expresses the basic tilt compensation principle of a tilted RTK receiver, which is actually a lever arm correction issue. The principle of tilt compensation is quite simple and straightforward, while challenges for high-precision tilted RTK positioning lie in

- robust and high-sensitivity tracking of GNSS signals particularly at large angles.
- rapid and accurate INS heading alignment for the low-cost IMU.
- maintaining the accuracy of the attitude matrix $\mathbf{C}_b^n$ at an acceptable level during the surveying period.

The first challenge is addressed by using the advanced signal tracking technologies, providing the maximum number of observations for tilt-compensated RTK solutions [1]. Therefore, we focus on addressing the other two problems in the present work.

2. Heading Alignment of the Low-cost INS

INS initial heading alignment challenges arise for a tilt-compensated RTK receiver as commonly encountered in other situations using low-cost INSs, such as low-cost GNSS/INS integrated navigation. Alignment, i.e., attitude initialization, is the process whereby the orientation of the axes of an INS is determined with respect to the reference axis system [6], e.g., the process of calculating the initial roll, pitch and heading angles. For a tilted RTK receiver, it is necessary to accomplish accurate INS alignment within a very short period of time, e.g., a few seconds, to achieve a rapid reaction. As analyzed in our previous work [11], the roll and pitch angles can be initialized quickly to sufficient accuracy even for a low-cost chip-level IMU. It is the heading initialization that poses the major difficulty in initial alignment, where a 1.15-2°-accuracy is typically required.

Our team proposed a novel method to address the INS heading alignment problem for the low-cost IMU embedded in tilt-compensated RTK receivers in [11]. In this section, we review and summarize the key points of the proposed method for the sake of article completeness.

The proposed INS heading alignment method involves a specific motion, as illustrated in the top panel of Fig 3: the pole tip is fixed at a ground point O, and the pole is then tilted to an arbitrary position A, after which it is shifted to another position B to finish the alignment motion. IMU and RTK measurements are simultaneously recorded. Such a simple but specific operation greatly benefits the algorithm design by regarding pole movement as rigid body motion with a fixed point. The corresponding data processing is characterized as follows:

(1) It is assumed that the initial heading angle of the IMU is zero. Then, the INS-indicated trajectory, i.e., the IMU center position history, is calculated using the gyro-derived attitude and pole length by treating the pole movement as the motion of a rigid body with a fixed point to enhance the trajectory accuracy.

(2) The RTK-indicated trajectory, i.e., the discrete IMU center position history, is obtained from the RTK receiver.

(3) The offset of the assumed initial heading angle in step (1) is then determined as the angle between the INS- and RTK-indicated position increment vectors in the horizontal direction based on the fact that the INS-indicated and RTK-indicated trajectories are similar in shape.

We have proven that the INS-indicated trajectory is similar to the true trajectory in shape but with a rotation due to an initial heading error, as:

$$\Delta\hat{\boldsymbol{r}}_I^n(t) = \mathbf{C}_n^{\hat{n}}\Delta\boldsymbol{r}_I^n(t) \tag{3}$$

$$\mathbf{C}_n^{\hat{n}} = \begin{bmatrix} \cos\Delta\psi & -\sin\Delta\psi & 0 \\ \sin\Delta\psi & \cos\Delta\psi & 0 \\ 0 & 0 & 1 \end{bmatrix} \tag{4}$$

where $\Delta\boldsymbol{r}_I^n(t)$ is the delta position vector, i.e. the position increment vector. Here, $\hat{\boldsymbol{r}}_I^n(t)$ denotes the computed INS-indicated quantity of $\Delta\boldsymbol{r}_I^n(t)$; $\Delta\psi$ is the initial heading error to be determined and can be computed, as illustrated in the bottom panel of Fig 3, by:

$$\cos\Delta\psi = \frac{\overline{A'B'}\cdot\overline{A'B''}}{\|\overline{A'B'}\|\cdot\|\overline{A'B''}\|} \tag{5}$$

In practice, to obtain the initial heading error, we should compute the INS-indicated and RTK-indicated trajectories, as depicted in Fig 3. Traditionally, the INS-indicated position is computed through the INS mechanization procedure, and the practical algorithm and implementation have been provided in many textbooks, such as [10]. Through this approach, the positioning solution tends to drift significantly even over a short period due to the large biases in both accelerometer and gyro measurements,

which degrade the accuracy of INS-indicated trajectories and, in turn, influence the initial heading estimation in the proposed method.

In the present work, we calculate the INS-indicated position in a new way to largely prevent its accuracy drift. It is clear that the pole movement in the alignment phase is a typical motion of a rigid body with a fixed point. The INS-indicated trajectory can be straightforwardly determined based on the gyro-derived pole attitude and the constant pole length. The INS-indicated position of the IMU center is calculated by equation (1) in its discrete time form as:

$$\boldsymbol{r}_I^n(t_k) = \boldsymbol{r}_T^n - \mathbf{D}_R^{-1}(t_k)\mathbf{C}_b^n(t_k)\boldsymbol{l}^b \tag{6}$$

where t_k denotes the discrete time instant and $\boldsymbol{r}_T^n$ and $\boldsymbol{l}^b$ are constant vectors known in advance. The attitude matrix $\mathbf{C}_b^n$ is updated from the start epoch by integrating the gyro measurement using the direction using the direction cosine matrix chain rules [10], as:

$$\mathbf{C}_{b(k)}^{n(k)} \approx \mathbf{C}_{b(k)}^{n} = \mathbf{C}_{b(k-1)}^{n}\mathbf{C}_{b(k)}^{b(k-1)} \tag{7}$$

$$\mathbf{C}_{b(k)}^{b(k-1)} = \mathbf{I}_3 + \sin\phi_k(\boldsymbol{u}_k\times) + (1-\cos\phi_k)(\boldsymbol{u}_k\times)^2 \tag{8}$$

$$\boldsymbol{\phi}_k = \Delta\boldsymbol{\theta}_k + \frac{1}{12}\Delta\boldsymbol{\theta}_{k-1}\times\Delta\boldsymbol{\theta}_k \tag{9}$$

where k denotes the time instant t_k; $\boldsymbol{\phi}_k$ is the rotation vector defining the frame b_k attitude relative to frame b_{k-1} at time t_k; ϕ_k is the length of $\boldsymbol{\phi}_k$; $\Delta\boldsymbol{\theta}_{k-1}$ and $\Delta\boldsymbol{\theta}_k$ are the incremental angle measurements of the IMU at t_{k-1} and t_k, respectively; $\boldsymbol{u}_k$ is the unit vector of the vector $\boldsymbol{\phi}_k$; $\boldsymbol{u}_k\times$ denotes the 3×3 skew symmetric matrix generated by the 3×1 vector $\boldsymbol{u}_k\times$; $\mathbf{I}_3$ is the 3×3 identity matrix.

In this new approach, only gyro measurements are used in computing the INS-indicated position or trajectory, as expressed by equation (6). Hence, the INS-indicated trajectory or positioning results are free of any accelerometer-associated errors and affected only by the gyro attitude drift error. Therefore, compared to the traditional strapdown INS mechanization approach, the new method is expected to greatly reduce the positioning errors.

3. RTK/INS Integration Aided by ZUPT

The attitude solutions tend to drift as long as the motion is not strong due to the weak observability of the heading errors even if the RTK position is updated. Here, we propose to use the ZUPT considering the lever arm compensation. This makes it easier to obtain ZUPT opportunities, and it is expected to enhance the positioning performance.

The IMU data and RTK positions are fused in a loosely coupled manner. The extended Kalman filter (EKF), which uses the position and velocity residual vectors along with the error models, is adopted to estimate the error state $\hat{\boldsymbol{x}}$, which is fed back into the INS to remove the estimated errors from the system and estimate the optimal attitude.

a) System Models

For this KF design, the error state is defined as:

$$\boldsymbol{x} = \begin{bmatrix}(\delta\boldsymbol{r}^n)^{\mathrm{T}} & (\delta\boldsymbol{v}^n)^{\mathrm{T}} & \boldsymbol{\phi}^{\mathrm{T}} & \boldsymbol{b}_g^{\mathrm{T}} & \boldsymbol{b}_a^{\mathrm{T}} & \boldsymbol{s}_g^{\mathrm{T}} & \boldsymbol{s}_a^{\mathrm{T}}\end{bmatrix}^{\mathrm{T}} \tag{10}$$

where $\delta\boldsymbol{r}^n = [\delta r_N, \delta r_E, \delta r_D]^{\mathrm{T}}$ are the position errors in meters in the directions north, east and down, respectively. This term is defined as the difference between the INS-indicated position vector $\hat{\boldsymbol{r}}^n$ and true position vector $\boldsymbol{r}^n$. Similarly, $\delta\boldsymbol{v}^n = [\delta v_N, \delta v_E, \delta v_D]^{\mathrm{T}}$ are INS velocity errors resolved in the *n*-frame. In addition, $\boldsymbol{\phi} = [\phi_r, \phi_p, \phi_h]^{\mathrm{T}}$ represent INS-indicated attitude errors in the *phi*-angle formulation [12], and ϕ_r, ϕ_p, and ϕ_h denote the error in the roll, pitch and heading angle, respectively. Finally, $\boldsymbol{b}_g$ and $\boldsymbol{b}_a$ are the residual bias of the gyroscope and of the accelerometer, respectively, and $\boldsymbol{s}_g$ and $\boldsymbol{s}_a$ are the residual scale factor errors of the gyroscope and of the accelerometer, respectively.

The filter design requires a differential equation describing the dynamics of the error state. In summary, the navigation filter system model in continuous time is given by

$$\dot{\boldsymbol{x}}(t) = \mathbf{F}(t)\boldsymbol{x}(t) + \mathbf{G}(t)\boldsymbol{w}(t) \tag{11}$$

where $\mathbf{F}(t)$ is the system dynamic matrix and $\mathbf{G}(t)$ is the process noise mapping matrix. Here, $\boldsymbol{w}$ denotes the process noise vector as

$$\boldsymbol{w} = \begin{bmatrix}\boldsymbol{w}_a^{\mathrm{T}} & \boldsymbol{w}_g^{\mathrm{T}} & \boldsymbol{w}_{gb}^{\mathrm{T}} & \boldsymbol{w}_{ab}^{\mathrm{T}} & \boldsymbol{w}_{gs}^{\mathrm{T}} & \boldsymbol{w}_{as}^{\mathrm{T}}\end{bmatrix}^{\mathrm{T}} \tag{12}$$

where $\boldsymbol{w}_a$ and $\boldsymbol{w}_g$ are the noise corrupting the accelerometers and gyros measurements, respectively. The inertial sensor biases and scale factor errors are modeled as a first-order Gauss-Markov process with driving noise $\boldsymbol{w}_{gb}$, $\boldsymbol{w}_{ab}$, $\boldsymbol{w}_{gs}$, and $\boldsymbol{w}_{as}$. To obtain the system model, the time derivative of each state variable must be calculated. The expanded form of matrix $\mathbf{F}$ and $\mathbf{G}$ can be found in [13].

To correct INS with external auxiliary information, the system measurement model is constructed. Distinctive from the previous algorithm, our filter is aided by ZUPT with lever arm compensation, and the measurement equation is displayed below:

$$\boldsymbol{z} = \mathbf{H}\boldsymbol{x} + \boldsymbol{e} \tag{13}$$

where $\boldsymbol{z}$ is the measurement vector; $\mathbf{H} = [\mathbf{H}_{\text{ZUPT}} \quad \mathbf{H}_r]^{\text{T}}$ is the design matrix including ZUPT with lever arm compensation denoted by $\mathbf{H}_{\text{ZUPT}}$ and RTK position update denoted by $\mathbf{H}_r$; and $\boldsymbol{e}$ is the measurement noise.

b) Measurement Models: ZUPT with Lever Arm Compensation

As shown in Fig 1, when a practitioner walks with the pole, it is very difficult to keep the pole with INS the absolutely still, whether when the pole is in the air or on the ground. At this time, the common ZUPT algorithm is not applicable. However, it is confirmed that when the tip lands, its velocity is zero, as shown in Fig 2. As a result, the zero-velocity information of the pole tip can be used to suppress the error divergence of the INS. The velocity of the INS can be linked to that of the tip by the lever arm measured in advance. Based on the difference between the measured velocity that equals zero and the estimated velocity of the tip, ZUPT can be carried out.

Based on the navigation result of the INS, estimating the velocity of the tip can be denoted as:

$$\boldsymbol{v}_T^n = \boldsymbol{v}_I^n - [(\boldsymbol{\omega}_{ie}^n\times) + (\boldsymbol{\omega}_{en}^n\times)]\,\mathbf{C}_b^n\boldsymbol{l}^b - \mathbf{C}_b^n(\boldsymbol{l}^b\times)\boldsymbol{\omega}_{ib}^b \tag{14}$$

where $\boldsymbol{v}_I^n$ and $\boldsymbol{v}_T^n$ are the velocity vectors of the IMU center and the pole tip in the *n*-frame , respectively; $\boldsymbol{\omega}_{ie}^n$ is the Earth's rotation rate vector in the *n*-frame; $\boldsymbol{\omega}_{en}^n$ denotes the transport rate vector, *i.e.*, the rotation rate vector of the *n*-frame with respect to the *e*-frame, where the calculation of $\boldsymbol{\omega}_{ie}^n$ and $\boldsymbol{\omega}_{en}^n$ can be found in [14, p.24]; $\boldsymbol{\omega}_{ib}^b$ is the body angular rate with respect to the inertial-frame measured by gyroscopes in the *b*-frame; $\mathbf{C}_b^n$ is the attitude transformation matrix from the *b*-frame the *n*-frame; $\boldsymbol{l}^b$ is the lever arm vector from the IMU center to the pole tip; and the 3-by-3 skew symmetric matrix $(\cdot\times)$ is so defined that the cross product satisfies $\boldsymbol{a}\times\boldsymbol{b} = (\boldsymbol{a}\times)\boldsymbol{b}$ for these two arbitrary vectors.

Introducing calculation errors into equation (14), we can obtain the equation of INS-indicated pole tip velocity, as:

$$\hat{\boldsymbol{v}}_T^n \approx \hat{\boldsymbol{v}}_I^n - [(\boldsymbol{\omega}_{ie}^n\times) + (\boldsymbol{\omega}_{en}^n\times)]\,\hat{\mathbf{C}}_b^n\boldsymbol{l}^b - \hat{\mathbf{C}}_b^n(\boldsymbol{l}^b\times)\hat{\boldsymbol{\omega}}_{ib}^b \tag{15}$$

where $\hat{\boldsymbol{v}}_T^n$ is the INS-indicated velocity vector of the pole tip; $\hat{\boldsymbol{v}}_I^n$ is the INS-indicated velocity vector of the IMU center; the errors in $\boldsymbol{\omega}_{ie}^n$ and $\boldsymbol{\omega}_{en}^n$ are ignored for simplicity; $\hat{\mathbf{C}}_b^n$ is the INS-indicated attitude transformation matrix, which satisfies $\hat{\mathbf{C}}_b^n = \mathbf{I} - (\boldsymbol{\phi}\times)$, where $\mathbf{I}$ is the 3-by-3 unit matrix; and $\hat{\boldsymbol{\omega}}_{ib}^b = \boldsymbol{\omega}_{ib}^b + \delta\boldsymbol{\omega}_{ib}^b$ is the error-containing body angular rate, where $\delta\boldsymbol{\omega}_{ib}^b = \boldsymbol{s}_g\cdot\boldsymbol{\omega}_{ib}^b + \boldsymbol{b}_g + \boldsymbol{w}_g$.

Substituting the error terms into equation (14) and discarding the second-order errors, we have:

$$\begin{aligned}\hat{\boldsymbol{v}}_T^n \approx\ & \boldsymbol{v}_T^n + \delta\boldsymbol{v}_I^n \\ & - (\boldsymbol{\omega}_{in}^n\times)(\mathbf{C}_b^n\boldsymbol{l}^b\times)\boldsymbol{\phi} - \mathbf{C}_b^n(\boldsymbol{l}^b\times\boldsymbol{\omega}_{ib}^b)\times\boldsymbol{\phi} \\ & - \mathbf{C}_b^n(\boldsymbol{l}^b\times)diag(\boldsymbol{\omega}_{ib}^b)\boldsymbol{s}_g - \mathbf{C}_b^n(\boldsymbol{l}^b\times)\boldsymbol{b}_g\end{aligned} \tag{16}$$

The measurement velocity of the pole tip can be expressed as:

$$\tilde{\boldsymbol{v}}_T^n = \boldsymbol{v}_T^n - \boldsymbol{e}_v \tag{17}$$

where $\tilde{\boldsymbol{v}}_{\text{tip}}$ is the measurement velocity of the pole tip, which is theoretically zero in the survey phase; and $\boldsymbol{e}_v$ is the measurement noise of velocity.

By subtracting the measurement velocity of the pole tip from its INS-indicated velocity, the measurement velocity vector can be obtained, as:

$$\begin{aligned}\boldsymbol{z}_v &= \hat{\boldsymbol{v}}_T - \tilde{\boldsymbol{v}}_T \\ &= \mathbf{H}_{\text{ZUPT}}\boldsymbol{x} + \boldsymbol{e}_v\end{aligned} \tag{18}$$

By substituting equation (16) and equation (17) into equation (18), the design matrix of ZUPT with lever arm compensation can be obtained as:

$$\mathbf{H}_{\mathrm{ZUPT}} = \begin{bmatrix} \mathbf{0}_3 & \mathbf{I}_3 & \mathbf{H}_1 & -\mathbf{C}_b^n(\boldsymbol{l}^b\times) & \mathbf{0}_3 & \mathbf{H}_2 & \mathbf{0}_3 \end{bmatrix} \tag{19}$$

where the two matrices, $\mathbf{H}_1$ and $\mathbf{H}_2$, are respectively defined by:

$$\mathbf{H}_1 = -(\boldsymbol{\omega}_{in}^n\times)(\mathbf{C}_b^n\boldsymbol{l}^b\times) - \left[\mathbf{C}_b^n(\boldsymbol{l}^b\times\boldsymbol{\omega}_{ib}^b)\times\right] \tag{20}$$

$$\mathbf{H}_2 = -\mathbf{C}_b^n(\boldsymbol{l}^b\times)\mathrm{diag}(\boldsymbol{\omega}_{ib}^b) \tag{21}$$

c) Measurement Models: RTK Position Update

In the other part of this paper, the IMU center is assumed to coincide with the GNSS APC for simplicity. Actually, the two positions cannot be perfectly coincident. Similar to equation (1), the relationship between the position of the GNSS APC and the IMU center is expressed as:

$$\boldsymbol{r}_A^n = \boldsymbol{r}_I^n + \mathbf{D}_R^{-1}\mathbf{C}_b^n\boldsymbol{l}_{GNSS}^b \tag{22}$$

where $\boldsymbol{r}_A^n$ is the position of the GNSS APC without error; $\boldsymbol{r}_I^n$ is the position of the IMU measurement without error; $\mathbf{D}_R^{-1} = \mathrm{diag}(\begin{bmatrix} \frac{1}{R_M+h} & \frac{1}{(R_N+h)\cos\varphi} & -1 \end{bmatrix}^{\mathrm{T}})$ is a diagonal matrix that converts the delta position from meter to delta latitude, delta longitude in radian and delta height in meters, where R_M and R_N are respectively the meridian and transverse radii of curvature; $\mathbf{C}_b^n$ is the attitude transformation matrix from *b*-frame to *n*-frame; and $\boldsymbol{l}_{GNSS}^b$ is the lever arm from the IMU center to the GNSS APC.

The calculation error from INS propagates in this position projection, as:

$$\hat{\boldsymbol{r}}_A^n = \hat{\boldsymbol{r}}_I^n + \hat{\mathbf{D}}_R^{-1}\hat{\mathbf{C}}_b^n\boldsymbol{l}_{GNSS}^b \tag{23}$$

where $\hat{\boldsymbol{r}}_A^n$ is the INS-indicated GNSS APC position; $\hat{\boldsymbol{r}}_I^n$ is the IMU center position computed by the INS; $\hat{\mathbf{D}}_R^{-1}$ is the unit transformation matrix $\mathbf{D}_R^{-1}$ with error; and $\hat{\mathbf{C}}_b^n$ is the error-containing attitude transformation matrix.

Now, the position of the GNSS APC from RTK positioning is used as position auxiliary information for INS correction. The measurement of the GNSS APC position can be shown as:

$$\tilde{\boldsymbol{r}}_A^n = \boldsymbol{r}_A^n - \hat{\mathbf{D}}_R^{-1}\boldsymbol{e}_r \tag{24}$$

where $\tilde{\boldsymbol{r}}_A^n$ is the GNSS APC position from RTK positioning, which contains errors due to the measurement noise; and $\boldsymbol{e}_r$ is the measurement noise.

The measurement vector is constructed by the difference between the INS-indicated GNSS APC position $\hat{\boldsymbol{r}}_A^n$ and the observed GNSS APC position $\tilde{\boldsymbol{r}}_A^n$, as:

$$\begin{aligned} \boldsymbol{z}_r &= \hat{\mathbf{D}}_R\left(\hat{\boldsymbol{r}}_A^n - \tilde{r}_A^n\right) \\ &= \mathbf{H}_r\boldsymbol{x} + \boldsymbol{e}_r \end{aligned} \tag{25}$$

where $\boldsymbol{z}_r = [\delta n \quad \delta e \quad \delta d]^{\mathrm{T}}$ is the measurement vector of position difference in meters in the directions north, east and down; $\hat{\mathbf{D}}_R$ is the inverse matrix of $\hat{\mathbf{D}}_R^{-1}$.

By substituting equation (23) and equation (24) into equation (25) and reorganizing the terms yiled, the design matrix of RTK position update can be expressed as

$$\mathbf{H}_r = \begin{bmatrix} \mathbf{I}_3 & \mathbf{0}_3 & \left(\mathbf{C}_b^n\boldsymbol{l}_{GNSS}^b\times\right) & \mathbf{0}_3 & \mathbf{0}_3 & \mathbf{0}_3 & \mathbf{0}_3 \end{bmatrix}^{\mathrm{T}} \tag{26}$$

4. Attitude Accuracy Requirement Analysis

Fig 1 intuitively explains the essence of tilted compensation as the position correction by means of tilt angle and horizontal azimuth measured by the IMU [14], as:

$$\begin{bmatrix} l_N \\ l_E \\ l_D \end{bmatrix} = \begin{bmatrix} l\sin\alpha\cos\beta \\ l\sin\alpha\sin\beta \\ -l\cos\alpha \end{bmatrix} \tag{27}$$

where l_N, l_E and l_D are the tilted corrections in the north, east, and upward directions, respectively; l is the length of the lever arm between the IMU center and the pole tip. Note that the tilt angle α and the horizontal azimuth β show pole attitude intuitionally. The IMU provide its own attitude angles, *i.e.*, heading ψ, pitch θ and roll ϕ. They are closely related and their relation is subsequently derived.

Recalling equation (1), the delta position vector $\boldsymbol{l}^b$ due to tilted compensation is computed in a straightforward manner as

$$\boldsymbol{l}^n = \mathbf{C}_b^n \boldsymbol{l}^b \tag{28}$$

where $\boldsymbol{l}^b = [0 \quad 0 \quad l]^{\mathrm{T}}$ is the lever arm vector resolved in the b-frame. Substituting the formulas (1) and (2) into (28), we have:

$$\begin{bmatrix} l_N \\ l_E \\ l_D \end{bmatrix} = \begin{bmatrix} -(s\phi s\psi + c\phi s\theta c\psi)\cdot l \\ -(c\phi s\theta s\psi - s\phi c\psi)\cdot l \\ -c\phi c\theta \cdot l \end{bmatrix} \tag{29}$$

Comparing equation (29) with equation (27), we obtain the transformation relation between angles α and β and the IMU attitude angles ψ, θ and ϕ as

$$\cos\alpha = \cos\phi\cos\theta, \quad (0 \le \alpha \le 90^\circ) \tag{30}$$

$$\tan\beta = \frac{-s\phi c\psi + c\phi s\theta c\psi}{s\phi s\psi + c\phi s\theta c\psi}, \quad (0 \le \beta \le 360^\circ) \tag{31}$$

The above two equations help us understand how the IMU's attitude errors affect the tilted RTK's horizontal and vertical position accuracy.

Considering that the computed IMU attitude angles contain errors, the computed tilt compensation can be written as

$$\hat{\boldsymbol{l}}^n = \hat{\mathbf{C}}_b^n \boldsymbol{l}^b \tag{32}$$

where $\hat{\boldsymbol{l}}^n$ denotes the computed delta position vector due to tilt compensation; $\hat{\mathbf{C}}_b^n$ is the computed attitude matrix, which contains errors due to the errors in roll, pitch and heading Euler angles and is written as follows [6]

$$\hat{\mathbf{C}}_b^n = [\mathbf{I} - \boldsymbol{\Psi}]\,\mathbf{C}_b^n \tag{33}$$

where $\mathbf{I}$ is the 3×3 identity matrix and $\boldsymbol{\Psi}$ is given by

$$\boldsymbol{\Psi} = \begin{bmatrix} 0 & -\delta\psi & \delta\theta \\ \delta\psi & 0 & -\delta\phi \\ -\delta\theta & \delta\phi & 0 \end{bmatrix} \tag{34}$$

where $\delta\phi$, $\delta\theta$, and $\delta\psi$ are the errors of roll, pitch and heading, respectively. The tilt compensation error, denoted by $\delta\boldsymbol{l}^n$, due to the errors in the computed attitude matrix is given by

$$\delta\boldsymbol{l}^n = \hat{\mathbf{C}}_b^n \boldsymbol{l}^b - \mathbf{C}_b^n \boldsymbol{l}^b \tag{35}$$

Substituting (33) into (35), we have:

$$\delta\boldsymbol{l}^n = -\boldsymbol{\Psi}\mathbf{C}_b^n \boldsymbol{l}^b \tag{36}$$

Substituting (34) and (2) into (36), we have:

$$\begin{bmatrix}\delta l_N\\ \delta l_E\\ \delta l_D\end{bmatrix} = \begin{bmatrix}\delta\psi(-s\phi c\psi + c\phi s\theta s\psi)l - \delta\theta(c\phi c\theta)l\\ -\delta\psi(s\phi s\psi + c\phi s\theta c\psi)l + \delta\phi(c\phi c\theta)l\\ \delta\theta(s\phi s\psi + c\phi s\theta c\psi)l - \delta\phi(c\phi s\theta s\psi - s\phi c\psi)l\end{bmatrix} \tag{37}$$

Equation (37) depicts the tilt compensation errors caused by the INS-indicated attitude errors $\delta\phi$, $\delta\theta$ and $\delta\psi$. We can determine the necessary tilt compensation errors induced by the heading errors as

$$\begin{bmatrix}\delta l_{N,\delta\psi}\\ \delta l_{E,\delta\psi}\\ \delta l_{D,\delta\psi}\end{bmatrix} = \begin{bmatrix}\delta\psi\cdot(-s\phi c\psi + c\phi s\theta s\psi)\cdot l\\ -\delta\psi\cdot(s\phi s\psi + c\phi s\theta c\psi)\cdot l\\ 0\end{bmatrix} \tag{38}$$

where $\delta l_{N,\delta\psi}$, $\delta l_{E,\delta\psi}$ and $\delta l_{D,\delta\psi}$ are respectively the north, east and vertical components of the $\delta\psi$-induced tilt compensation errors in the horizontal direction.

Then, the horizontal position error is given by:

$$\begin{aligned}\delta l_{plane,\delta\psi} &= \sqrt{(\delta l_{N,\delta\psi})^2 + (\delta l_{E,\delta\psi})^2}\\ &= \delta\psi\cdot l\cdot\sqrt{1 - c^2\phi c^2\theta}\end{aligned} \tag{39}$$

Substituting (30) into (39) yields

$$\delta l_{plane,\delta\psi} = \delta\psi\cdot l\cdot\sin\alpha \quad (0 \le \alpha \le 90^\circ) \tag{40}$$

Similarly, we can obtain the effects of $\delta\phi$ and $\delta\theta$ as

$$\delta l_{plane,\delta\phi} = \delta\phi\cdot l\cdot\cos\alpha \quad (0 \le \alpha < 90^\circ) \tag{41}$$

$$\delta l_{plane,\delta\theta} = \delta\theta\cdot l\cdot\cos\alpha \quad (0 \le \alpha < 90^\circ) \tag{42}$$

$$\delta l_{height,\delta\phi} = \delta\phi\cdot(\sin\alpha\sin\beta)\cdot l \tag{43}$$

$$\delta l_{height,\delta\theta} = -\delta\theta\cdot(\sin\alpha\cos\beta)\cdot l \tag{44}$$

Considering equations (39)-(44), we see that the heading accuracy influences the accuracy of the horizontal position only. The roll (or pitch) accuracy has an impact on both the horiaontal and the vertical directions. Actually, the incluence in the vertical direction is very weak, so we discuss only the horizontal direction. Suppose that the length of the pole is 2 m and the required precision in the horizontal direction is 2 cm. Fig 5 plots the attitude accuracy requirement for different tilt angles. We observe that the heading accuracy needs to be improved as the tilt angle increases gradually. For example, when the pole is tilted to 10°, a 3.3° heading accuracy is adequate, but for a larger tilt angle, such as 30°, the heading accuracy should be raised to 1.15°. Different from the heading, the larger the tilt angle is, the lower the accuracy requirement for the roll (or pitch). The variation magnitude of the roll (or pitch) curve is smaller than that of the heading curve. In practice, the tilt angle is usually within 30°, and then a 1.15° heading and a 0.66° roll (or pitch) are needed to guarantee a 2 cm horizontal accuracy. A 0.66° roll (or pitch) is easy to acquire, while a 1.15° heading is harder to achieve. To realize valid tilt compensation, emphasis should be placed on the heading determination.

III. EXPERIMENT AND RESULTS

To validate the feasibility and evaluate the performance of the proposed algorithms, numerous tests were conducted, and the details are shown as follows. Take one of the field tests as an example. The test was carried out under open-sky conditions on a campus playground to provide GNSS receivers with favorable observation circumstances. A MEMS GNSS/INS integrated system and two geodetic GNSS receivers were used for data collection, and a quasitactical grade GNSS/INS integrated system was applied to provide reference heading values. The MEMS GNSS/INS integrated system, i.e., INS-Probe, was developed by the Navigation Group of the GNSS Research Center at Wuhan University. In this system, Invensense ICM-20602, a dollar-level IMU chip, is integrated and synchronized with a built-in GNSS receiver card from u-blox. Two high-quality GNSS receivers from Trimble Inc. were employed to perform RTK positioning. The independent reference system, termed M39, was a GNSS/INS integrated system from Wuhan MAP Space Time Navigation Technology, Ltd., China. It integrates a quasitactical grade IMU, ADIS16488 from Analog Devices Inc. (ADI), with a NovAtel OEM-7 receiver card from NovAtel Inc., Canada.

Fig 4 shows a photograph of the experimental setup and illustrates how the sensors were connected. An aluminum plate was fixed on the top end of a Trimble carbon fiber pole, the INS-Probe, and M39, and the antennas were firmly mounted on the plate. A switch is attached on the pole tip to identify the motions of touching ground. Thus, we can know the right time to enable ZUPT in data processing. Table 2 lists the main specifications of the equipment, and more information on the equipment is listed below:

- IMU: Invensense ICM-20602, a dollar-level MEMS IMU.
- GNSS rover receiver: a Trimble NetR9 GNSS receiver.
- GNSS base station receiver: a Trimble NetR9 GNSS reference receiver.
- Independent reference: M39, which has been proven to provide an independent integrated heading reference accurate to 0.1° in postprocessing.
- GNSS antenna: NovAtel GPS-702-GGL, and a u-blox ANN-MB multiband GNSS antenna.

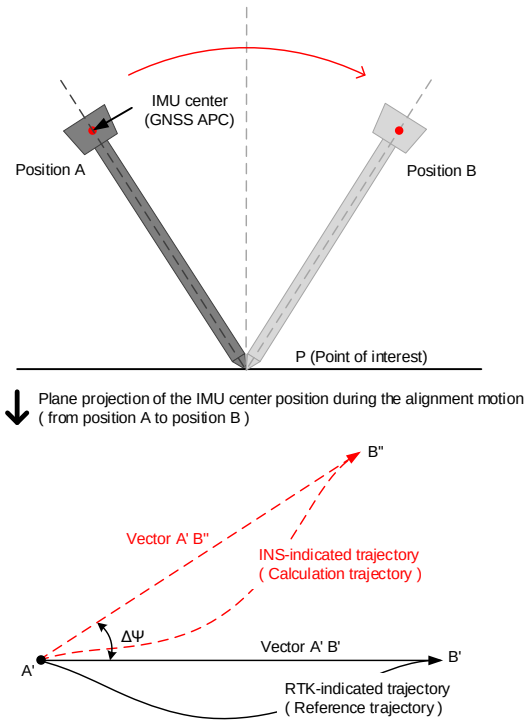

Figure 3: Illustration of the proposed INS alignment principle for tilt-compensated RTK receivers.

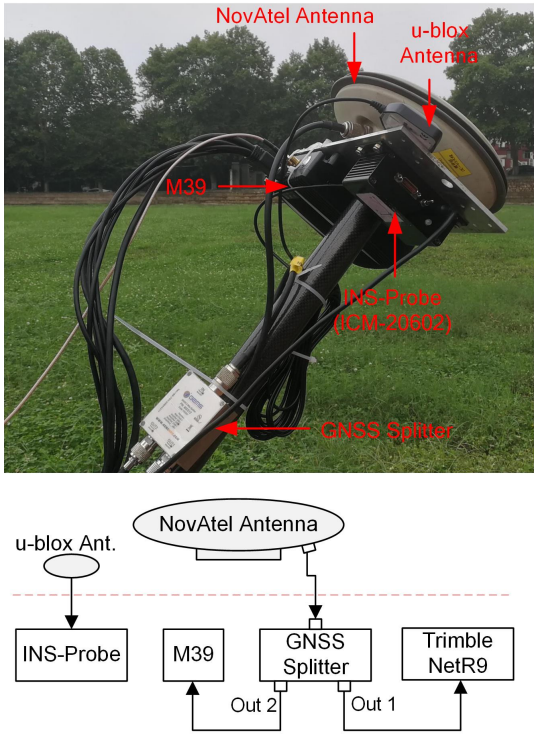

Figure 4: Photograph of the experimental setup. The rover Trimble Net R9 receiver is not shown in the upper image.

The baseline between the rover receiver and base station is approximately 1000 m. The offset from the IMU center to the pole tip is 2.1 m. Both INS-Probe and M39 recorded synchronized IMU data at 200 Hz. The two Trimble receivers recorded 1 Hz raw GNSS data simultaneously to allow for carrier phase-based differential GNSS positioning processing. To fully test the proposed heading alignment algorithm and the completely tilted RTK solution, the test was conducted by two independent schemes: an alignment test and a tilted RTK test.

In the alignment test, datasets were collected during four independent sessions according to the following procedure:

(1.1) Fix the pole tip on a given point (denoted as point P) on the ground, tilt the pole with a given tilt angle α at an arbitrary position A, and remain stationary for approximately 3 seconds, to determine the initial roll and pitch angles.

(1.2) Shift the pole around point P from position A to another position B within 2 seconds or 3, with the tilt angle initially reduced and then increased to approximately α, as illustrated in Fig 3.

(1.3) Repeat steps (1.1) and (1.2) approximately 200 times to obtain multiple alignment samples under the given tilt angle α.

(1.4) Repeat steps (1.1) to (1.3) for α = 15°, 30° and 45° to evaluate the performance of the proposed alignment algorithm under the different tilt angles.

(1.5) Restart the sensors, and repeat steps (1.1) to (1.4) to collect data in four different sessions.

Step (1.2) is the complete alignment operation needed for the proposed algorithm, which we call the alignment sample. Therefore, each session contains approximately 600 alignment samples (200 samples under each tilt angle), and the whole alignment experiment contains approximately 2400 alignment samples.

In the tilted RTK test, datasets were collected during nine independent sessions according to the following procedure:

(2.1) Fix the pole tip at a given point i on the ground, hold the pole vertically, and perform normal RTK measurement for 90 s to obtain the reference position of point *i*.

(2.2) Perform the alignment operation on point *i* according to steps (1.1) and (1.2) with a tilt angle of 30°. Repeat the alignment operation 10 times.

(2.3) Keep the pole tip fixed on point *i*, and shift the pole in all directions at the same tilt angle α for approximately 60 s; thus, the horizontal direction are circles centered at point *i*.

(2.4) Repeat step (2.3) for α = 15°, 30°, 45° and 60° to evaluate the performance of the proposed tilted RTK solution under the different tilt angles.

(2.5) Change the ground point i, and repeat steps (2.1) to (2.4) to collect data in nine different sessions (i = 1, 2, $\cdots$ 9).

In step (2.2), redundant alignment operations are needed in case of failure in the previous alignment. Steps (2.3) and (2.4) compose the tilted measurement operation to test the performance in different directions and at different tilt angles.The top view of the experimental trajectory in one session shows four concentric circles with different radii. We denote an epoch's measurement as a tilted RTK measurement sample.

1. Data Processing

The reference results are calculated as follows. The IMU and GNSS data from M39 are postprocessed in a loosely coupled model with a Rauch-Tung-Striebel (RTS) smoother to provide a heading reference that was proven accurate to 0.1°. The GNSS data during the traditional RTK survey period from the base station and rover receivers are processed in the carrier phase-based differential positioning mode by combining the forward and reverse filtering solutions to provide the reference position of the points to be surveyed.

Heading alignment data processing is conducted using the data collected from the alignment test. In every alignment sample, the longest pair of vectors (in the INS-indicated trajectory and RTK-indicated trajectory) is used to obtain an approximate initial heading. Then, a least square estimator is implemented to obtain an optimal result. More details about alignment processing can be found in our previous work [11].

Tilted RTK data processing is conducted using the data collected from the tilted RTK test. This starts from the heading alignment using the data collected by alignment motions. When the alignment is carried out successfully, a reasonable heading is applied to loosely coupled integration aided by ZUPT with lever arm compensation. This heading is processed in forward filtering as the tilted RTK works in real-time mode. Finally, the GNSS/INS attitude is used for tilt compensation to obtain the position history of the pole tip, and the position errors are calculated relative to the reference position.

2. Results Analysis

a) Accuracy of the Initial Heading Estimates

It has been proven that, to reach a certain precision requirement, different tilt angles in the survey phase require different alignment accuracies, as shown in Fig 5. For example, for a 2 m pole, to obtain 2 cm tilt compensation accuracy, 1.15° alignment accuracy is required when the pole is tilted to 30° and 3.30° alignment accuracy is required when the pole is tilted to 10°. In general, a large tilt angle is avoided, and the pole is tilted smaller than 30° in survey, thus a 1.15° alignment accuracy is favorable. Fig 6 depicts the distribution of the heading alignment errors, which is approximately a Gaussian distribution. The RMS of the heading alignment errors is 0.49°, and 98.2% of the samples are within 1.15°. The Leica tilted RTK receiver GS18 can achieve a 2° accuracy within 10 s under sufficient motion. From this comparison, we can conclude that the proposed alignment method is sufficiently accurate for the tilted RTK receiver and is a much more time-efficient method than the conventional alignment methods.

When we sort the heading alignment error sequences in ascending tilt angle order, we see that there is no notable upward trend when the tilt angles are smaller than 30°. A slight uptrend is shown when the tilt angles are larger than 30°. We know that a

large tilt angle is unfavorable for tilted surveys but has a mixed impact on heading alignment. This is because a large tilt angle can provide longer position increment vectors, which benefits the initialization; however, worse performance of the receiver and more prominent instrument errors of the IMU are also inevitable.

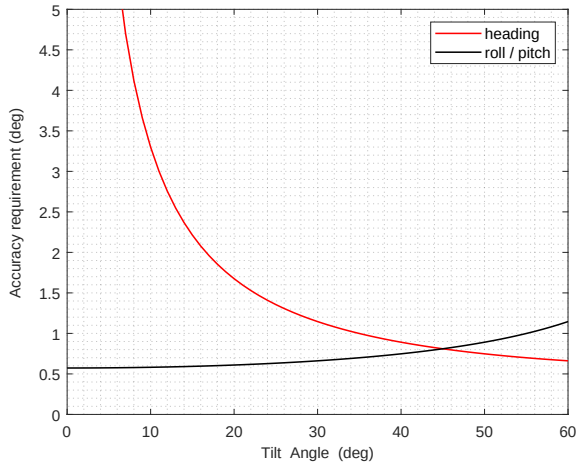

Figure 5: The attitude accuracy requirement for different tilt angles when pole length is 2 m and the horizontal position accuracy is 2 cm.

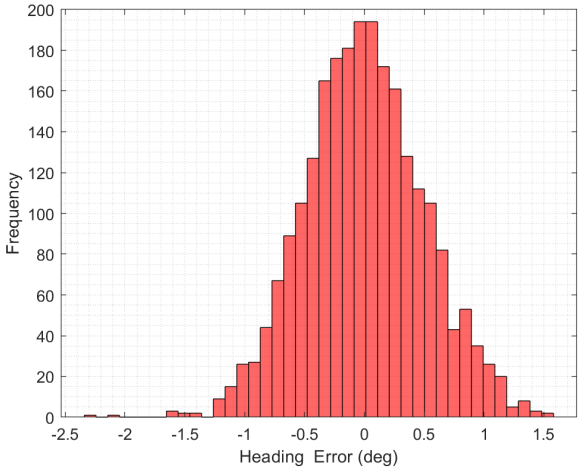

Figure 6: Distribution of the initial heading errors of 2400 samples.

b) Effect of ZUPT with Lever Arm Compensation

ZUPT with lever arm compensation reduces the cumulative errors of the INS by validating the zero velocity of the pole tip. The effect is remarkable when comparing the calculation results with and without ZUPT. Fig 7 gives the top view of the position errors of tilted RTK with ZUPT compensation from one session. Most points are distributed around an ordinate origin with a radius of 2.5 cm. Fig 8 shows the top view of the position errors of tilted RTK without ZUPT. The error margin is widened more clearly than results with ZUPT depicted in Fig 7, with an east error of up to 5.79 cm, a north error of up to 6.60 cm, and the maximal horizontal position error reaching 6.85 cm. Here, 70% of points are distributed within a 2.5 cm radius. Other points are spread out and mainly distributed within a 5.0 cm radius, which is twice the ZUPT compensation mode.

Fig 9 depicts the position errors (horizontal and vertical) of the tilted RTK solution with and without ZUPT in ascending tilt angle order. The top shows the horizontal errors. In the first 700 test cases in which the tilt angles are below 30°, both error curves climb slowly with increasing tilt angle, but the results without ZUPT show a larger error and stronger upward trend. In the test cases ranging from 700 to 1800, there is no significant uptrend in the position error as the tilt angle increases. However, greater error dispersion is shown, indicating that the tilted RTK solution is less stable when the tilted angles range from 30° to 60°. ZUPT can usefully constrain the error fluctuation to some degree. In the test cases ranging from 1800 to 2400 when the tilt angles are lager than 60°, the errors without ZUPT rise sharply and even exceed 6 cm. At such a large tilt angle, the ZUPT compensation mode shows prominent advantages, of which errors can be kept within 3 cm. More details about horizontal error are given in Table 1. In practice, a horizontal error within 2 cm is desirable; thus, we take the ratio of error within 2 cm as a criterion. The statistical results show that ZUPT can usefully raise this ratio at even at a large tilt angle range. Note that even with ZUPT assistance, the advanced horizontal position accuracy is still not perfect for practical measurement at a large tilt angle larger than 30°. The reason is that the effects of the algorithms are limited at a large tilt angle and that the signal tracking technology of GNSS receivers in tilt mode is necessary.

The bottom subfigure of Fig 9 plots the vertical position errors. Distinctive from the horizontal errors, the vertical errors show relatively high amplitude fluctuations. In the first 700 test cases, the error standard deviations of tilted RTK without and with ZUPT are 0.73cm and 0.64 cm, respectively, which are larger than those in the horizontal direction. The results without ZUPT have a more abrupt change than the results with ZUPT. In the test cases ranging from 700 to 1400 when the tilt angles range from 30° to 45°, the two error curves show little difference, and the ZUPT compensation mode even performs worse. In the test cases ranging from 1400 to 2400, the vertical errors are disperse and larger than the results with smaller tilt angles. ZUPT compensation at a large tilt angle brings a very modest stability improvement. A comparison of the top subfigure of Fig 9 indicates that ZUPT compensation is less effective in the vertical direction. This is because 1) larger noise is associated with the vertical GNSS RTK positioning; 2) in the field test, the plastic surface of the playground where the pole tip is fixed tends to cave in. This phenomenon causes an uncertain variation in the vertical position. The vertical velocity of the pole tip is not exactly zero, which is not desirable for ZUPT.

Table 1: Statistics of the horizontal position error over different tilt angles α.

Tilt Angle (°)	Max (cm)		STD (cm)		$\delta \boldsymbol{r}_{plane} \leq 2cm$ Ration (%)	
	ZUPT×	ZUPT✓	ZUPT×	ZUPT✓	ZUPT×	ZUPT✓
≤ 30	3.13	2.72	0.57	0.40	87.25	96.97
$30 \sim 45$	3.78	3.25	0.81	0.64	60.23	78.36
$45 \sim 60$	4.18	3.57	0.77	0.68	78.83	86.66
≥ 60	8.23	3.16	1.40	0.53	36.72	95.64

c) Position Errors of the Proposed Tilted RTK Solution

Fig 10 depicts the position errors (horizontal and vertical) and tilt angles of the 2389 samples in the nine sessions from the tilted RTK test. In the third subplot, the variation in tilt angle shows nine cycles, with each cycle containing four phases: approximately 15°, 30°, 45° and 60°. It is clear from this curve that in each session of the tilted RTK test, the pole was tilted over four different angles. The corresponding position error increases as the tilt angle increases, with horizontal errors over 3.6 cm and vertical errors near 5.7 cm at a large tilt angle. Fig 11 depicts the distribution of the north error (top) and east error (bottom). The RMS of the north error and the east error are 0.99 cm and 0.92 cm, respectively.

Recalling Fig 9 where we sort the position error sequences in ascending tilt angle order, we can observe the correction between position errors and tilt angles. The performance of the tilted RTK becomes poorer with increasing tilt angle, manifested in a large position error and lower stability. The reasons for this phenomenon may be twofold, as explained in the introduction section: 1) The RTK positioning accuracy decreases with increasing tilt angle due to the smaller elevation angle of the incoming GNSS signal. In our receivers, no additional advanced signal tracking technology was adopted. 2) As the tilt angle increases, the impact of the uncompensated gyro scale factor and cross-coupling errors becomes more notable; therefore, the tilt compensation accuracy declines. In practical tilted surveys, a large tilt angle is usually avoided. The proposed tilted RTK solution can achieve a 2 cm horizontal position accuracy at a 96.97% confidence level with a normal tilt angle smaller than 30°. This indicates that this new approach could competently serve as a feasible solution for tilted GNSS RTK.

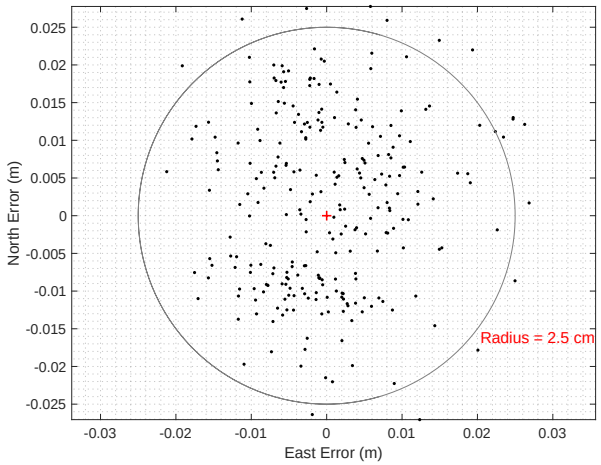

Figure 7: Top view of the position errors of tilted RTK with ZUPT compensation with tilt angles ranging from 10° to 60° in a session.

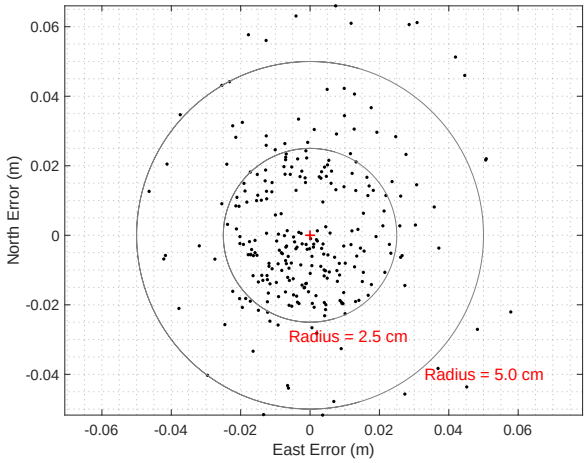

Figure 8: Top view of the position errors of tilted RTK without ZUPT compensation with tilt angles ranging from 10° to 60° in a session.

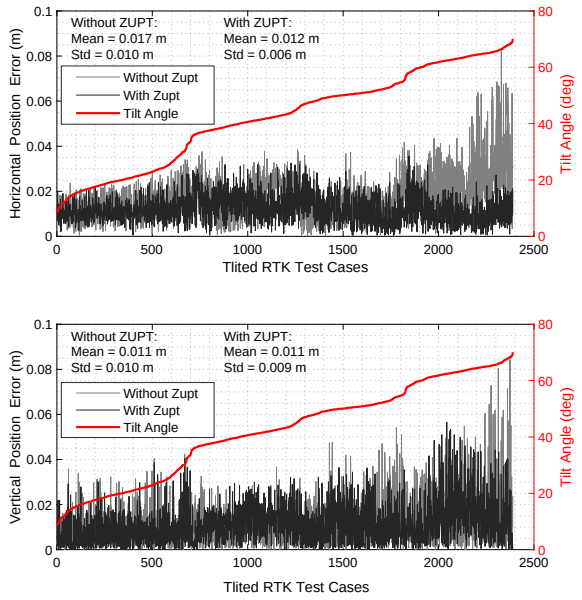

Figure 9: Position errors (horizontal and vertical) with and without ZUPT in ascending tilt angle order.

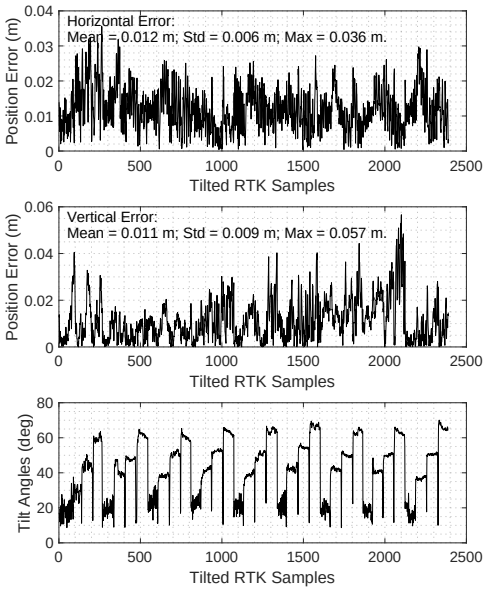

Figure 10: Position errors and corresponding tilt angles in the nine different sessions of the tilted RTK test.

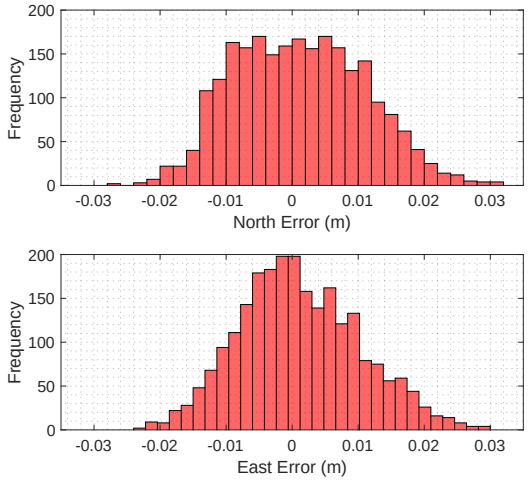

Figure 11: Distribution of the horizontal position errors of the proposed tilted RTK solution.

Table 2: Specifications of the key equipment.

Equipment	Specifications
M39	• Data rate: IMU 200 Hz, GNSS 1 Hz • Gyroscope performance Input range: $\pm$450 deg/s In-run bias stability: 6 deg/h Angular random walk: 0.3 deg/$\sqrt{\text{h}}$ • Accelerometer performance Range: $\pm$18 g In-run bias stability: 0.1 mg Velocity random walk: 0.029 m/s/$\sqrt{\text{h}}$
ICM-20602	• Size: 3 mm$\times$3 mm$\times$0.75 mm • Data rate: 200 Hz • Gyroscope noise: 0.24 deg/$\sqrt{\text{h}}$ • Accelerometer noise: 100 μg/$\sqrt{\text{Hz}}$
Trimble NetR9	• Sampling rate: up to 50 Hz (configurable) • RTK surveying performance Horizontal:8 mm + 1 ppm RMS Vertical:15 mm +1 ppm RMS
GPS-702-GGL	• Signals tracked: GPS L1/L2, GLONASS L1/L2, L-band, BDS B1, Galileo E1

IV. CONCLUSION

Tilted RTK solutions have been developed rapidly in recent years. However, academic reports are limited and technical details are not readily avaliable. Focusing on the present technical problems, this paper devises a low-cost and efficient tilted RTK solution, including a heading alignment method and ZUPT with lever arm compensation in a GNSS/INS integrated filter. Note

that the navigation parameters (especially the heading) tend to diverge when the surveyor changes points and the pole is in the air. There are three strategies in our solution to help convergence: 1) integrating GNSS with INS; 2) enabling ZUPT with lever compensation if the pole tip touchs ground; 3) performing alignment motions when the heading accuracy cannot meet the requirement. Field tests are carried out numerous times to obtain reliable statistical results. It is proven that a 1.15° accuracy at a 98.2% confidence level in initial heading determination can be easily achieved within only 2 to 3 seconds by the proposed method. When taking the ratio of error within 2 cm as a criterion, ZUPT with lever arm compensation can raise this ratio effectively even at a large tilt angle. The accuracy of the proposed tilted RTK solution is up to 2 cm at a 96.97% confidence level with a normal tilt angle (<30°), which indicates that this new approach could competently serve as a feasible solution for tilted GNSS RTK.

There are some remaining problems in this study. First, the quality control is inadequate. In the present work, reference values from postprocessing and empirical values are adopted to evaluate parameters. This method is not feasible and reliable. Second, the mounting angles are not estimated, and the error analysis of mounting angles have not been studied. We obtain the mounting angles by grid search in postprocessing. A precise calibration method or reliable estimation method is desiderable. Therefore, to achieve a more comprehensive tilted RTK solution, furture study in the above questions should be made.

ACKNOWLEDGEMENTS

The author would like to thank Dr. Qijin Chen and Dr. Xiaoji Niu, who provided the supervision and support needed for this work. And the author would like to thank Dr. Tisheng Zhang and Hailiang Tang in the research group for providing the MEMS INS module. In addition, the author would like to thank Changxin Lai and Ruonan Guo for their assistance in the experiments. This work was supported in part by the National Key Research and Development Program of China (No.2016YFB0501803) and the National Natural Science Foundation of China under Grant 41904019 and Grant 41674038.

REFERENCES

[1] X. Luo, S. Schaufler, M. Carrera, and I. Celebi, "High-precision RTK positioning with calibration-free tilt compensation," in *FIG Congress 2018*, 6th to 11th May 2018, Conference Paper.

[2] B. M. Scherzinger, "Ains enhanced survey instrument," 2009.

[3] K. Li and Y. Chen, "Analysis of high precision RTK tilt measurement technologies," in *China Satellite Navigation Conference, CSNC2019*, 22nd to 25th May 2019, Conference Paper.

[4] X. Luo, S. Schaufler, and B. Richter, "Leica GS18 T world's fastest GNSS RTK rover," Switzerland, 2018.

[5] M. Wu, Y. Wu, X. Hu, and D. Hu, "Optimization-based alignment for inertial navigation systems: Theory and algorithm," *Aerospace Science & Technology*, vol. 15, no. 1, pp. 1–17, 2011.

[6] D. H. Titterton and J. L. Weston, "Strapdown inertial navigation technology," 2004.

[7] Y. Wu and X. Pan, "Velocity/position integration formula part i: Application to in-flight coarse alignment," *IEEE Transactions on Aerospace & Electronic Systems*, vol. 49, no. 2, pp. 1006–1023, 2011.

[8] Groves and D. Paul, "Principles of gnss, inertial, and multisensor integrated navigation systems, 2nd edition [book review]," *IEEE Aerospace & Electronic Systems Magazine*, vol. 30, no. 2, pp. 26–27, 2015.

[9] G. Chang, T. Xu, Q. Wang, S. Li, and K. Deng, "Gnss attitude determination method through vectorization approach," *IET Radar Sonar & Navigation*, vol. 11, no. 10, pp. 1477–1482, 2017.

[10] P. G. Savage, "Strapdown inertial navigation integration algorithm design part 1: Attitude algorithms," *Journal of Guidance, Control, and Dynamics*, vol. 21, no. 1, pp. 19–28, 1998.

[11] Q. Chen, H. Lin, R. Guo, and X. Niu, "Rapid and accurate initial alignment of the low-cost MEMS IMU chip dedicated for tilted RTK receiver," *GPS Solutions*, vol. 24, no. 4, pp. 1–13, 2020. [Online]. Available: http://dx.doi.org/10.1007/s10291-020-01032-8

[12] E. H. Shin, "Estimation techniques for low-cost inertial navigation," Thesis, 2005.

[13] X. Niu, Q. Zhang, L. Gong, C. Liu, H. Zhang, C. Shi, J. Wang, and M. Coleman, "Development and evaluation of GNSS/INS data processing software for position and orientation systems," *Survey Review*, vol. 47, no. 341, pp. 87–98, 2015.

[14] J. Lixin, Y. Songlin, and C. Xinhuan, "Study on the characters of random error caused by antenna rod slant for gps rtk surveying," *Railway Survey*, 2002.